Infrared Spectroscopic Properties of Sodium Bromide Aerosols

Lorena Miñambres, María N. Sánchez, Fernando Castaño, and Francisco J. Basterretxea*

Departamento de Química Física Facultad de Ciencia y Tecnología Universidad del País Vasco/Euskal Herriko Unibertsitatea Campus de Leioa B. Sarriena, s/n Leioa 48940, Spain

Received: October 24, 2007; Revised Manuscript Received: April 3, 2008

The infrared extinction spectra of aqueous NaBr aerosols at ambient temperature have been measured as a function of relative humidity. Submicron-sized aerosol particles atomized from aqueous NaBr solutions at various concentrations are dried and/or mixed with nitrogen at different humidities and spectroscopically monitored as they flow through an infrared absorption cell. Estimated dry particle median diameters range from 0.24 to 0.15 μm, as calculated from Mie extinction theory. Measured deliquescence and efflorescence relative humidities (35−40% and 25−30%, respectively) are in accordance with previously reported ones. Our results show that NaBr particles take up water only moderately over the deliquescence point, with a significant increase at relative humidities above 70%. The effect of particle size onto water uptake properties has been studied, indicating that smaller particles take up lower amounts of water, and only increase their size significantly at relative humidities near saturation. Particle composition and diameter growth factors have been calculated from spectral data and are shown to be consistent with those predicted from thermodynamic data and Köhler theory. Band centers of liquid water in NaBr aerosols relative to pure water are blue-shifted up to 50 cm^{-1} at low humidities. Particle structure and phase, together with atmospheric implications, are also discussed.

Introduction

Atmospheric aerosols are important components of the Earth's atmosphere. They play a major role in the physical and chemical processes of the atmosphere, affecting issues such as air quality, visibility degradation, radiation forcing and climate change. Among naturally suspended particulate matter in the troposphere, sea salt aerosols constitute the second most abundant type after dust aerosol, and are the dominant aerosol species by mass above the oceans.[1] Ocean wave action is the primary mechanism for sea salt aerosol injection into the atmosphere, where residence times range from days to weeks. Sodium chloride is the principal component of sea salt, and weight percentages of its major components are the following:[1] Cl (55.04%), Na (30.61%), SO_4^{2-} (7.68%), Mg (3.69%), Ca (1.16%), K (1.1%) and Br (0.19%).

Tropospheric sea salt particles have highly reactive surfaces that undergo heterogeneous chemistry. Sodium chloride is known to participate in a variety of heterogeneous chemical reactions, specially with nitrogen oxides, which convert NaCl into $NaNO_3$ with the release of chlorine, which can further react with other atmospheric species.[2,3] Despite bromide ions being a minor component of seawater (and hence of sea salt particles), with roughly 650 mol of chloride per mol of bromide, bromine plays a notable role in tropospheric sea salt chemistry. There is clear evidence that sea salt is the source of bromine atom precursors generated in the gas phase and that their photolysis initiates chain reactions that lead to polar tropospheric ozone destruction via its reaction with Br atoms.[2,4] The rate of bromine atom production in the lower polar troposphere at polar sunrise has been estimated to be 3 or 4 orders of magnitude higher than atomic chlorine, a phenomenon known as "bromine explosion".[2] Recent laboratory studies[5,6] and field observations[7] have further addressed the atmospheric relevance of the reactivity of aqueous NaCl/NaBr salt solutions and aerosols. In a series of calculations involving NaCl and NaBr aerosol particles and gaseous OH or O_3, Thomas et al.[8] showed that interface processes involving surface Cl^- ions and gas-phase OH species are the main source of $Cl_2(g)$. In the case of Br^- ions, $Br_2(g)$ from OH(g) is formed mainly in the bulk aqueous phase and transferred across the interface. In contrast, the reaction of surface Br^- with $O_3(g)$ at the interface was found to be the primary source of $Br_2(g)$ under dark conditions.

Sea salt aerosols can take up significant amounts of water, exhibiting deliquescence and efflorescence properties under atmospheric conditions.[9] Water uptake by sea salt aerosols containing NaCl and NaBr is well-known to modify particle physicochemical properties and reactivity. The significance of bromine in heterogeneous chemistry is enhanced by the fact that, in mixtures of NaCl and NaBr, on exposure to water, bromide segregates to salt surface, increasing Br/Cl molar ratio by more than one order of magnitude.[10,11]

There has been abundant laboratory work on phase transitions of atmospheric marine salts,[9] with NaCl often being used as a surrogate for natural aerosols in studies of physicochemical properties. Different techniques have been employed to study the influence of relative humidity (RH) on NaCl studies, such as aerosol infrared spectroscopy,[12–14] single crystal infrared spectroscopy,[15,16] differential mobility analysis,[17] single particle levitation,[18] or atomic force microscopy.[19] Fewer studies have been reported on NaBr. Myerson et al.[20,21] reported efflorescence studies of highly supersaturated $NaBr/H_2O$ solutions by employing an electrodynamic levitator trap technique. Snyder and Richardson[22] studied the solution to solid-phase transition of various systems, including NaBr with pure and mixed water solvents and methanol using levitated microscopic particles in a quadrupole trap. In a series of papers, Cohen and coworkers[23–25] investigated concentrated electrolyte solutions, among them

* Corresponding author. Phone: +34 94 601 2532. Fax: +34 94 601 3500. E-mail address: franciscojose.basterretxea@ehu.es.

10.1021/jp710268r CCC: $40.75
Published on Web 06/28/2008

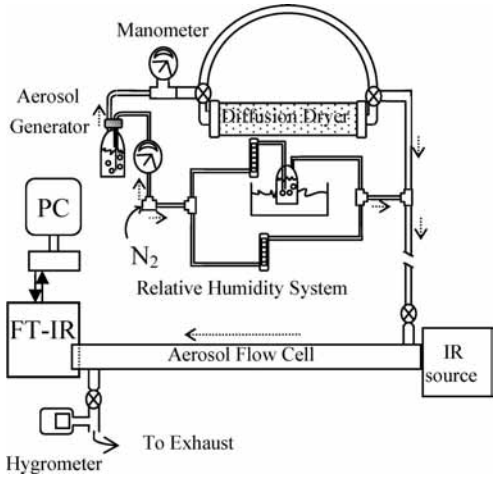

Figure 1. Setup of the experimental system.

NaBr, suspending single, 20 μm diameter charged droplets of aqueous salt solutions using an electrodynamic balance. They obtained several thermodynamic properties, such as water activities for single and mixed electrolyte solutions, and solute nucleation. For NaBr/H_2O systems, they also obtained a deliquescence RH of 45% and an efflorescence RH of 22% for anhydrous salt. Recently, Wise et al.[26] studied the hygroscopic behavior of 0.1−4 μm diameter single salt particles (including NaBr) with a transmission electron microscope equipped with an environmental cell, obtaining results in agreement with those of Cohen et al. So far, there are no reported studies of hygroscopic properties of NaBr/H_2O system in aerosols.

This work reports a study of the hygroscopic properties of NaBr aqueous aerosols by infrared absorption spectroscopy in an aerosol flow cell. The aim is to analyze the detailed behavior of particles as a function of the relative humidity, to understand particle water content as humidity varies. Particle hygroscopic behavior has also been monitored as a function of particle size, showing appreciable water uptake differences for different particle diameters, specially at higher values of RH.

Experimental Section

Figure 1 sketches the experimental arrangement used. NaBr aerosols were prepared by dissolving solid NaBr (Alfa Aesar, 99% purity) into deionized water at concentrations of 0.142, 0.0142 and 0.00142 kg/L. The solution is drawn into a commercial constant output atomizer (TSI 3076), in which pure N_2 (Praxair, 99.990%) is injected at 2.5 bar, yielding a high velocity jet and atomizing the liquid. Large droplets are removed by impact on the walls and only submicrometer aerosol particles leave the atomizer, following a distribution that will be assumed to be lognormal. Droplet median diameter can be varied by evaporating the solvent.

The formed aerosol flow either enters or bypasses a diffusion drier (TSI 3062) and is subsequently injected into a 1 m long, 50 mm diameter infrared glass absorption cell at ambient temperature. Aerosol flow through the cell can be easily visualized by eye or by passing a He−Ne laser beam through the cell. The flow is seen to be uniform through the whole cell, except at the inlet, where turbulent behavior is apparent. To control the relative humidity, a flow of N_2 (Praxair 99.990%) is divided in two, with one going through a water bubbler to provide water vapor saturated nitrogen and the other kept dry. The bubbler was immersed in a thermostated bath between 25 and 30 °C to increase the water vapor pressure. Both flows are subsequently mixed together prior to being added to the aerosol. Flows in both lines are measured with rotameters and are adjusted with needle valves to get the desired RH values. The sum of both flows was kept constant, to keep aerosol concentration unchanged. RH values were measured by inserting the sensor of a digital thermohygrometer (Hanna HI93640N) into the central section of the flow exiting the aerosol cell. We were able to vary the RH value from about 3% (only dry N_2 flow) to 98% (only humid N_2 flow). The aerosol cell and tubing had to be cleaned frequently to remove salt deposits that absorb substantial quantities of water vapor and preclude achieving of high RH values. With this configuration, two kinds of experiments were conducted: one in deliquescence mode, in which dessicated particles were mixed with nitrogen flow with increasing RH, and another in efflorescence mode, in which aerosols bypassing the dessicator are mixed with nitrogen flow with decreasing RH. To check that mixing of humid nitrogen flow with aerosol was not limited by the length of the tube connecting the mixing zone with the aerosol cell, deliquescence and efflorescence measurements were carried out using tubes of different lengths (2.6 and 7.5 m). The results show no appreciable difference between both sets of experiments.

An infrared source (ORIEL 6580) mounted inside an Apex illuminator (ORIEL 66450) gives collimated infrared radiation that goes lengthways through the aerosol cell, which has CaF_2 windows at its ends. The outcoming radiation is directed to an MCTA infrared detector mounted in a Fourier transform infrared spectrometer (Nicolet Magna 860) that records an extinction spectrum from 1100 to 4000 cm^{-1}. Sample interferograms were averaged by collecting typically 200 scans at 4 cm^{-1} resolution. The infrared optical path is sealed and flushed by a current of dry air to reduce ambient water infrared absorption. Background spectra are recorded before aerosol spectra with the aerosol cell evacuated by a rotary diaphragm pump. Although it was not possible to completely eliminate water vapor infrared absorption lines, signal intensity fluctuations are of the order of $\pm$0.007 in absorbance, as measured by comparing different averaged background spectra (200 scan average).

Spectra of water vapor flowing through the aerosol cell at selected RH values (measured with the hygrometer) were recorded to produce a calibration curve for the gaseous water integrated absorption (measured from 2166 to 1188 cm^{-1} in the H_2O bending ν_2 fundamental band) versus RH. In this way the RH in the aerosol cell can additionally be determined by measuring the integrated absorbance of water vapor and the aid of the calibration curve. Interference from particle absorption and scattering in the 2166−1188 cm^{-1} integration range were eliminated by subtracting particle spectra to obtain a zero baseline.

Results and Discussion

(A) NaBr Aerosol Extinction Spectra. Figure 2 shows two examples of NaBr aerosol extinction spectra obtained after atomizing the 0.142 kg/L solution and subtracting gaseous water absorption. The upper trace, obtained when aerosol bypasses the diffusion drier, shows a broad intense band with a maximum at 3380 cm^{-1} and a weaker one with a maximum at 1643 cm^{-1}, both assignable to liquid water. The pronounced baseline slope from lower to higher wavenumbers is due to the scattering of light by the particles. In the lower spectrum, corresponding to dried aerosol, liquid H_2O absorption has almost completely vanished, although a small signal centered at 3442 cm^{-1} can be seen, blue-shifted 62 cm^{-1} relative to nondessicated aerosols. The baseline slope is also considerably weaker, suggesting a

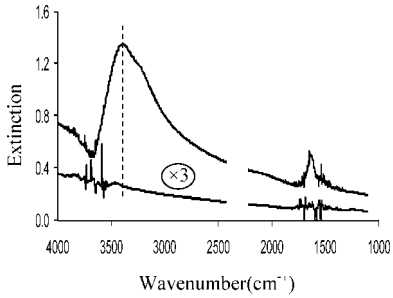

Figure 2. Infrared extinction spectra of NaBr aqueous aerosols generated from a 0.142 kg/L solution. The upper curve corresponds to undried particles, as they are formed in the atomizer; the lower curve (at magnified scale) shows particles passed though a diffusion drier. The narrow lines correspond to water vapor absorption, which have not been completely eliminated. The blank region around 2300 cm^{-1} corresponds to CO_2 absorption, which has been deleted for clarity. The dashed line has been included to help visualize the bandshift between dried and undried aerosols.

negligible scattering contribution in this region consistent with the formation of smaller particles. In both spectra, narrow lines are due to residual water vapor absorption lines, which remain after subtraction. The blank region in both spectra around 2300 cm^{-1} corresponds to CO_2 absorption, which has been eliminated for clarity. As expected, in these spectra no band can be assigned to the salt, indicating its complete ionization.

(B) Calculation of Particle Diameter Distribution from Mie Scattering Theory. Although we cannot directly measure the particle size distribution, it is useful to estimate the particle sizes at different RH's. The intensity F of light after travelling a distance z into an aerosol layer is given by $F = F_0 \exp(-b_{ext}z)$, where b_{ext} is the frequency-dependent extinction coefficient (cm^{-1}), which consists of two components, namely scattering and absorption: $b_{ext} = b_{scat} + b_{abs}$. For polydisperse particles, these coefficients can be calculated by the following formula:[27,28]

$$b_X = \sum_i \frac{\pi D_i^2}{4} N_i Q_{X,i} \quad (1)$$

where X stands for extinction, scattering or absorption, D_i is the particle diameter, N_i is the number density of particles with diameter D_i, and the sum extends over the different diameters present in the sample. $Q_{scat,i}$ and $Q_{ext,i}$ are the scattering and extinction efficiencies of the particles, respectively. They are quantities that depend on particle diameter, radiation wavelength, and the real (n) and imaginary (k) components of the particle's refractive index, which in turn depend on wavelength. For spherical particles, Q_{scat} and Q_{ext} can be computed exactly using Mie theory.[27]

We have calculated b_{scat} and b_{ext} for NaBr particles, taking optical constants from Li[29] (solid) and Rhine et al.[30] (4 M aqueous solutions). For solid NaBr, k can be taken to be zero from 1000 to 4000 cm^{-1} (i.e., solid NaBr particles will not absorb light in this region). The computation method proceeds as follows: for a given wavenumber, Q_{scat} and Q_{ext} are calculated for assumed spheres with different diameters using expressions given elsewhere.[27] N_i is computed assuming a lognormal distribution of particles with median diameter $\bar{D}_g$, geometric standard deviation σ_g, and total particle number density N. We have divided the lognormal distribution into 100 intervals, choosing the diameter interval to include more than 99.9% of the particles.[13] Next, b_{scat} and b_{ext} for each wavenumber are calculated using (1). The absorption coefficient is obtained simply by difference using $b_{abs} = b_{ext} - b_{scat}$ and the calculations were carried out at many wavenumbers to yield the $b(\nu)$ spectrum.

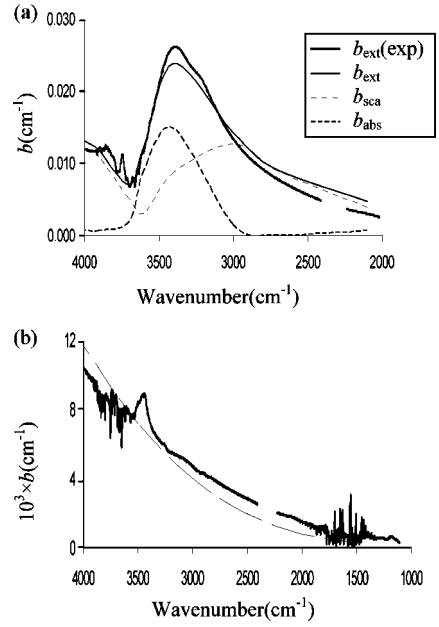

Figure 3. (a) Experimental extinction coefficient, b_{ext}(exp), vs wavenumber for undried NaBr particles formed from a 0.142 kg/L solution, together with b_{ext} calculation that give the best fit to experimental points. Calculated scattering and absorption coefficients b_{sca} and b_{abs} are also shown. (b) Experimental extinction spectrum (solid line) for dried NaBr particles formed from a 0.142 kg/L solution, together with scattering coefficient calculation (dashed line) that gives the best fit.

The infrared extinction spectra of aerosols can be used to determine particle properties by a retrieval method involving least squares fitting.[31] These properties include the number density, size distribution, and chemical composition. We have iteratively changed the parameters N, $\bar{D}_g$ and σ_g in our calculations to obtain the best fit to aerosol experimental spectra. Initial values of $N = 2 \times 10^6$ part/cm^3 and $\sigma_g = 1.8$ were taken, in accordance with atomizer specifications. Figure 3a shows one example in which both experimental and best fit calculated extinction spectra are shown for undried NaBr particles generated from the 0.142 kg/L solution along with calculated scattering and absorption components. For this case, the fitted parameters $N = 1.9 \times 10^6$ part/cm^3, $\bar{D}_g = 0.76$ μm and $\sigma_g = 1.74$ are obtained. Although particle median diameter will vary with RH, it is reasonable to assume that N and σ_g will remain constant for our experimental conditions.

The median diameter of dried particles (which exhibit only a scattering spectrum) can be obtained by fitting calculated and experimental scattering spectra, and fixing the previosuly obtained N and σ_g. Figure 3b shows a plot of the computed b_{sca} in the 1000−4000 cm^{-1} range for solid NaBr particles, together with the dried aerosol spectrum generated from the 0.142 kg/L NaBr solution. The fitting yields a dry particle median diameter of $\bar{D}_{g,0} = 0.24$ μm. Even though the agreement between experimental and calculated spectra in Figure 3 is reasonably good, some discrepancies can be observed. Fitted values around the maximum of the extinction curve in Figure 3a are lower than experimental ones, whereas the calculated extinction shows higher values than experimental ones below 3000 cm^{-1}. Also the scattering curvature in Figure 3b cannot be entirely reproduced. One reason for the differences in undried particles can be that optical constants used in the calculations correspond

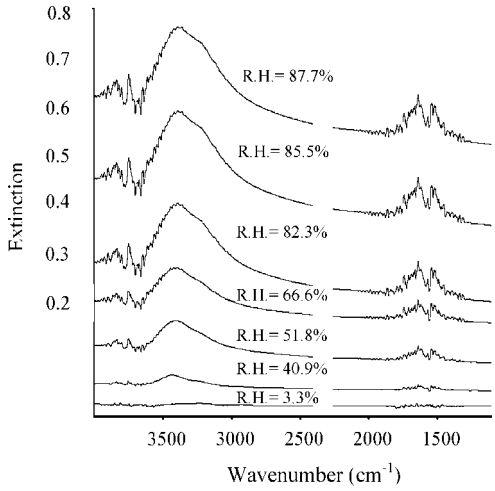

Figure 4. Infrared extinction spectra of NaBr aerosols generated from a 0.142 kg/L solution for a number of RH's in a deliquescence mode experiment. Vertical scales of different spectra have been offset for clarity.

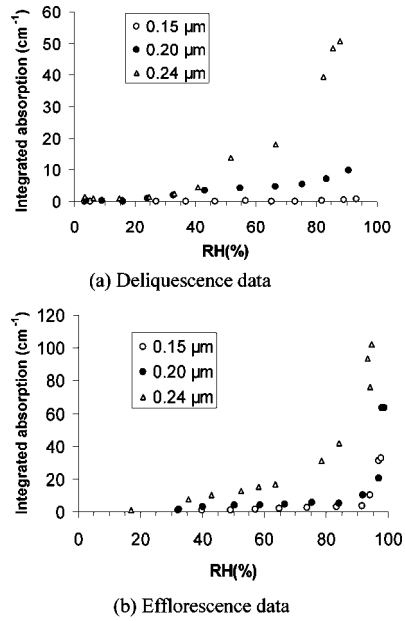

Figure 5. Integrated absorption values of liquid water from 2800 to 3600 cm^{-1} in NaBr aqueous aerosols generated from 0.142, 0.0142 and 0.00142 kg/L solutions (corresponding to particle median average diameters of 0.24, 0.20 and 0.15 μm, respectively) in deliquescence and efflorescence mode as a function of relative humidity (RH).

to 4 mol/L NaBr solutions, whereas NaBr aerosol concentration corresponding to Figure 3a is actually higher, as later shown in the paper. The error in fitting wet particles will also influence computed $\bar{D}_{g,0}$ for dry particles in Figure 3b, for which N and σ_g have been fixed. An additional source of error in dry aerosol calculations will probably be that particles are not expected to be uniform spheres, and corresponding Mie scattering calculations will not yield exact results.[27]

The previous procedure has been applied to spectra generated from 0.0142 and 0.00142 kg/L solutions. These solutions are 10 and 100 times more dilute than the original one, leading to smaller particles after passing through the diffusion drier. For dried particles generated from these solutions, the best agreements between Mie calculations and extinction spectra are obtained for $\bar{D}_{g,0}$= 0.20 μm (corresponding to the 0.0142 kg/L solution) and 0.15 μm (0.00142 kg/L solution). The information obtained by Mie scattering calculations constitutes the basis for several magnitudes calculated in the present work, such as liquid water integrated absorption, particle composition and growth factors. Although the absolute values of these quantities will be slightly affected by the outlined possible errors in retrieving particle distribution parameters, the variation of particle properties with relative humidity and the difference in behavior between small and big particles are not expected to change substantially.

(C) Variation of Liquid Water Absorbance with Relative Humidity. Figure 4 shows a series of extinction spectra for $\bar{D}_{g,0}$= 0.24 μm particles recorded in deliquescence mode. The spectra show that water uptake by aerosols is weak below 40% RH, as indicated by the size of the liquid water absorption band around 3400 cm^{-1}, which grows for higher RH values. Liquid water integrated band absorption from 2800 to 3600 cm^{-1} was calculated from these spectra as a measure of particle water content. Plots of integrated absorption versus RH for spectra recorded in deliquescence and efflorescence modes are shown in Figure 5, for particles formed from 0.142, 0.0142 and 0.00142 kg/L solutions, corresponding to $\bar{D}_{g,0}$= 0.24, 0.20 and 0.15 μm particles, respectively. Integrated band absorbances are computed by subtracting the scattering component to the recorded infrared extinction spectra. The absorption part will dominate in small particles, but scattering will be substantial for bigger ones. On the basis of our Mie scattering calculations, we have determined the relative contribution of scattering to extinction at each relative humidity and have corrected the measured extinction values to convert them to absorption spectra and finally obtain integrated band absorbances. As an example, Figure 3a shows the comparison between extinction and absorption spectra for undried aqueous particles from the 0.142 kg/L solution.

Figure 5 shows that $\bar{D}_{g,0}$= 0.24 μm particles in deliquescence mode are almost dry until RH = 35−40% and take up water pronouncedly at higher RH's. Therefore, the deliquescence RH can be located roughly at 35−40%, in agreement with other previously reported values.[23,26] In efflorescence mode, liquid particles readily lose water at high RH's (95−85%), and reach comparable integrated absorbances to deliquescent particles down to about 50% RH, where particles have lost most of their initial water. From this RH down, particles lose water at slower pace than the corresponding increase in deliquescent mode, becoming completely dried at roughly 25−30% RH. Thus the efflorescence RH can be located at 25−30%, also in agreement with published data.[23,26] From these results, it can be concluded that the hysteresis effect is not very marked.

To analyze the deliquescence/efflorescence behavior of aerosol particles with particle size, liquid water integrated absorption for $\bar{D}_{g,0}$= 0.20 and 0.15 μm aerosols are also shown in Figure 5. The main difference is that initially smaller particles take up less water. In the deliquescence experiment, for the smallest particles, liquid water absorption is nearly absent for RH up to 90%; i.e., the particles do not take up water even at high humidites. In the efflorescence experiment (Figure 5b), where higher RH's were obtained, $\bar{D}_{g,0}$ = 0.15 and 0.20 μm particles start with a high water content at RH near saturation, and lose water very abruptly at RH $\approx$ 95%, remaining nearly dry for RH < 90%, although there is a residual water content that slowly decreases with decreasing RH. The effect is much more accentuated than for the $\bar{D}_{g,0}$= 0.24 μm particles, in which water is being lost more gradually from RH = 90% to 30%. Although the sensitivity of our measurements is not sufficient to characterize precise values of deliquescence and efflorescence RH for the smaller particles, no indication of change with

particle size is apparent from our data (Figure 5). This is in agreement with the results from other authors.[26] We additionally mixed $\bar{D}_{g,0} = 0.15$ μm dessicated particles (from the 0.00142 kg/L solution) with a humid flow of nitrogen (at RH $\sim$ 86%) and retained them in a static mode inside the cell over 60 min. Infrared spectra recorded over that time interval show virtually no liquid water signal, indicating that dry particles are stable at high RH's. As particles formed from the 0.00142 kg/L solution are very small, particle loss by sedimentation is not substantial for the time period of 60 min. The presence of the particles inside the tube through all time was verified by the scattering produced by a He−Ne laser.

(D) Aerosol Composition. The liquid water content of the aerosols is obtained from their infrared absorption spectra. The Beer−Lambert law may be written as[28]

$$\tilde{A} = \frac{\bar{\sigma} N(H_2O) z}{2.303 \times 10^2} \quad (2)$$

where $\tilde{A}$ is the integrated band absorbance (cm^{-1}), $\bar{\sigma}$ is the integrated absorption cross section per molecule (m $molecule^{-1}$), $N(H_2O)$ is the number of H_2O molecules per unit volume of aerosol sample (molecules m^{-3}), and z is the optical path length (m). The integrated absorption cross section can be calculated as[27,28]

$$\bar{\sigma} = \frac{4\pi \times 10^4}{p} \int_{band} k \bar{\nu}\, d\bar{\nu} \quad (3)$$

where p is the molecular density of the bulk material (molecules m^{-3}), k is the imaginary part of the refraction index, and $\bar{\nu}$ the wavenumber (cm^{-1}). The integral extends over the OH asymmetric stretch absorption band (in our case, from 2800 to 3600 cm^{-1}). Although it is best to use k of NaBr aqueous solutions,[30] a rough estimate may be obtained from pure water data[32] with $\bar{\sigma} = 1.3 \times 10^{-18}$ m $molecule^{-1}$. With the previous data and the computed values of $\tilde{A}$ in the preceding section, we calculate $N(H_2O)$ for different values of RH. For example, at RH = 80% for $\bar{D}_{g,0} = 0.24$ μm particles, the calculation gives 7.1×10^{21} H_2O molecules m^{-3}.

To determine the NaBr solute content of the aerosols, a filter was inserted at the exit of the flow tube to collect dry aerosol particles in a given time interval. A membrane vacuum pump was used to increase the flow. The NaBr dry mass w deposited onto the filter after a time t is $w = JM_s t$, where J is the aerosol flow rate (m^3/min) and M_s the solute mass per unit volume of aerosol (kg/m^3). Thus weighing the solid mass deposited at the filter, together with J and t measurements, allows M_s to be calculated. During a time interval of 25 min, for the $\bar{D}_{g,0} = 0.24$ μm particles, 38 $\pm$ 2 mg of dessicated NaBr were collected at the aerosol tube exit. The aerosol flow was 7 L/min, as measured in a much more diluted NaBr solution because particles from concentrated solutions rapidly obstructed the filter and stopped the flow. Thus $M_s = 2.17 \times 10^{-7}$ kg/L, or 1.28×10^{21} molecules m^{-3} of aerosol. Combining the previous value with the liquid water content, the average overall composition of aerosol particles (as a function of RH) can be readily calculated. For example, at 80% RH for $\bar{D}_{g,0} = 0.24$ μm particles, m(NaBr) = 10.1 mol/kg. The quantity M_s remains constant in all measurements, but $N(H_2O)$ varies with relative humidity, thus altering particle composition.

Figure 6 depicts particle composition vs RH data for $\bar{D}_{g,0} = 0.24$ μm particles. Both deliquescence and efflorescence data are plotted together. Figure 6a collects the particle solute molar fractions obtained by the above method, and Figure 6b shows the variation of the ratio (moles of H_2O)/(moles of NaBr) for the same aerosols. The values in Figure 6a are compared with calculated ones from water activities of NaBr electrolyte solutions as a function of solute molality, taken from the thermodynamic data given by Cohen et al.[23]

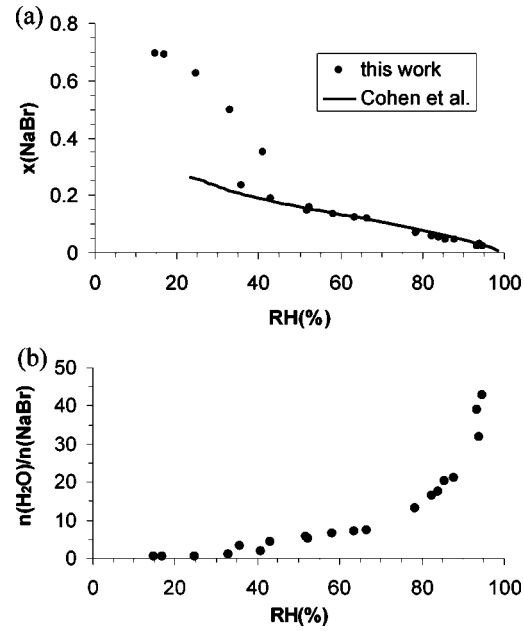

Figure 6. (a) NaBr aqueous particle molar fraction versus RH for $\bar{D}_{g,0} = 0.24$ μm diameter particles. The solid line is computed from data in ref 23. (b) Same composition data expressed as the ratio (moles of H_2O)/(moles of NaBr).

Our results agree with those by Cohen et al. for RH > 40% (i.e., at lower molalities), which roughly corresponds to the maximum NaBr molality for which their data are applicable.[23] The solubility of NaBr in cold water is 116 g NaBr per 100 cm^3 of water,[33] which corresponds to x(NaBr) = 0.17. Higher NaBr mole fractions in our measurements will presumably correspond to a mixture of solid salt and saturated solution.

(E) Growth Factors and Comparison with Köhler Theory Predictions. The above results have been used to calculate the particle growth factors defined as

$$g(RH) = \frac{D(RH)}{D_0} \quad (4)$$

where D(RH) is the particle diameter in humid air and D_0 is the volume equivalent diameter of solid particle. We have estimated the particle median diameter from our Mie scattering/extinction calculations, and computed the growth factor for spherical particles as $g(RH) = \bar{D}_g(RH)/\bar{D}_{g,0}$, where $\bar{D}_{g,0} = 0.24$, 0.20 or 0.15 μm, and $\bar{D}_g$(RH) has been determined for each measured RH. Figure 7 shows the particle growth factors as a function of RH for the three dry median diameters.

From Figure 7, initially smaller particles ($\bar{D}_{g,0} = 0.15$ and 0.20 μm) experience a diameter increase from 1 to 1.6 for RH's up to about 90%, the lower values for 0.15 μm particles; from this point the particles experience a very fast growth, in the region of unstability.[1] For the initially biggest particles ($\bar{D}_{g,0} = 0.24$ μm), the growth factors increase from 1.4 (at RH = 35%) to 2.4 (at RH = 90%), which are substantially higher than those of the smaller particles previously studied.

The above results are in overall agreement with the general trend predicted by Köhler.[1] Köhler curves are usually plotted as RH (or supersaturation) versus aqueous particle wet diameter. These curves are the result of two effects: the Kelvin effect, which favors the increase of vapor pressure (or RH), and the

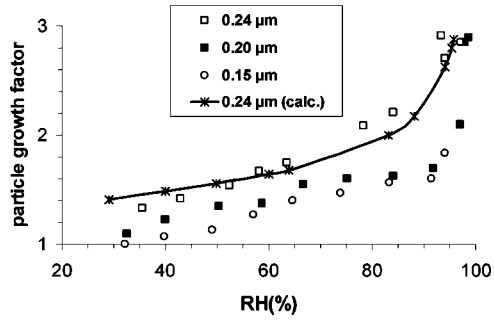

Figure 7. Experimental and calculated growth factors g(RH) for NaBr aqueous particles. Experimental values for $\bar{D}_{g,0} = 0.15$, 0.20 and 0.24 μm diameter particles were calculated by estimating the wet particle median diameters from Mie calculations. Computed values for $\bar{D}_{g,0}=$ 0.24 μm diameter particles (joined by a solid line) are based on thermodynamic data[34–36] and Köhler theory.

solute effect, which decreases it. The solute effect is associated with the high increase in RH with droplet diameter, and it depends on the mass of the initially dry particle. $\bar{D}_{g,0}= 0.15$ and 0.20 μm particles are expected to show steeper increases in RH with particle diameter than the $\bar{D}_{g,0}= 0.24$ μm particles. That is precisely the effect observed in our results of Figure 7, which are plotted the opposite way: smaller dry particles experience smaller growth factors with RH than bigger dry particles. Only at very high RH values do all the growth factors match (at $g \approx 3$), in the region of unstable equilibrium states, where particles grow out of control.

To check for the consistency of our previous results of g(RH), based on particle diameter determination by Mie calculations, we compare them with the predictions of Köhler theory using thermodynamic data.[34–36] To calculate the relationship between RH and the equilibrium diameter of a droplet, Köhler theory gives the following expression for the relative humidity:

$$\mathrm{RH}\ (\%) = 100 a_w \exp\left(\frac{4M_w\sigma_{sol}}{RT\rho_w D}\right) \quad (5)$$

where a_w, M_w and ρ_w are water activity, molar mass, and density, respectively, σ_{sol} is the surface tension of solution, and D the droplet diameter. The growth factor of a spherical particle, defined in (4), is computed as

$$g = \left(\frac{100\rho_s}{c_{sol}\rho_{sol}}\right)^{1/3} \quad (6)$$

where ρ_s and ρ_{sol} are salt and solution density, respectively, and c_{sol} is solution concentration (in mass percent). After calculating g(RH) from (6) at fixed ρ_s, ρ_{sol}, and c_{sol}, D(RH) is computed from (4), given a value for D_0. Finally, we calculate RH from (5). We thus obtain the g(RH) theoretical particle growth curve.

The following relevant data for NaBr solutions have been taken from the literature: density of water,[33] solid NaBr density,[37] density of aqueous NaBr solutions at 20 °C,[37] surface tension of sodium bromide aqueous solutions,[38] surface tension of liquid water[1] and activity of water in NaBr solutions.[23] Thermodynamic data are available for molalities up to 20 mol/kg, for which $a_w = 0.2328$. As $a_w \approx$ RH/100 (the exponential term in (5) is very close to 1 for the particles in this work), our calculations have not been extended to lower RH's. Also the available data for NaBr solution surface tension apply to molalities up to 3 mol/kg, although in this case it is feasible to extrapolate the surface tension assuming a linear relationship. Although the relationship will not be rigorously linear, it is expected that deviations will not substantially affect the results.

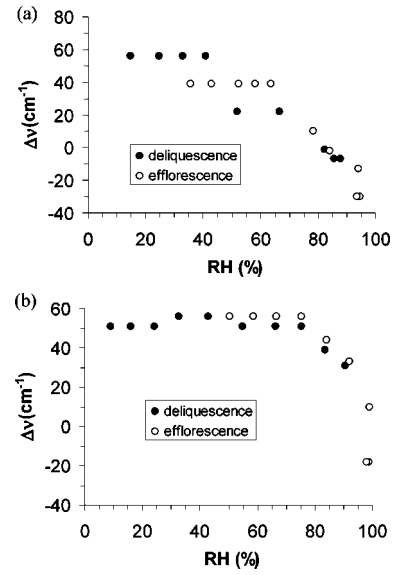

Figure 8. Band center shift of NaBr aqueous aerosols relative to pure liquid water, $\Delta\nu = \nu$(aerosol) $- \nu(H_2O)$. Data are shown in deliquescence and efflorescence modes. In (a) the aerosol was formed from a 0.142 kg/L NaBr solution, whereas in (b) the solution was 0.0142 kg/L.

This hypothesis is based on the data available for surface tension of NaCl aqueous solutions.[39]

A calculated g(RH) curve is shown in Figure 7 for solution data corresponding to the $\bar{D}_{g,0}= 0.24$ μm particles, the only system for which we directly measured solute concentrations. The agreement for g(RH) derived from Mie calculations and Köhler theory is, on the whole, satisfactory, taking into account the assumptions made in both sets of measurements.

(F) Liquid Water Absorption Bandshifts. We have measured the band center wavenumbers of the liquid water extinction band around 3400 cm^{-1} as a function of relative humidity for $\bar{D}_{g,0} = 0.24$ and 0.20 μm particles (absorption signals were too weak to get significant data for $\bar{D}_{g,0} = 0.15$ μm particles). Figure 8 shows the measured wavenumber shift $\Delta\nu = \nu$(aerosol) $- \nu(H_2O)$, where ν(aerosol) is the water extinction band center in NaBr aqueous aerosols and $\nu(H_2O)$ the band center in pure liquid water located at 3392 cm^{-1}.[32] In both deliquescence and efflorescence spectra, the general trend is that band center goes to higher wavenumber as RH decreases. No noticeable maximum displacement was observed for the liquid water band at 1600 cm^{-1}.

Figure 8 shows that, for $\bar{D}_{g,0} = 0.24$ μm particles in deliquescence mode, the band center shift is kept roughly constant at $\Delta\nu = +55$ cm^{-1} for RH below 40%. At higher RH, there is a gradual shift to lower wavenumbers, attaining -10 cm^{-1} at RH = 85%. A similar behavior is observed for $\bar{D}_{g,0} =$ 0.24 μm particles in efflorescence mode, with shifts of -30 cm^{-1} at humidities near saturation and shifting steadily towards $+40$ cm^{-1} at RH = 60%, with no further variation at lower RH. For $\bar{D}_{g,0} = 0.20$ μm particles, in both deliquescence and efflorescence measurements, band center shift is roughly constant at $+55$ cm^{-1} for RH between 10% and 75%. At higher relative humidities, the band center shifts to lower wavenumbers, with a steep transition at RH near saturation observed in the efflorescence curve. In all the experiments, at relative humidities close to saturation, the water absorption main band is accompanied by the appearance of a sideband in the extinction spectrum located at 3220 cm^{-1}, i.e., 150 cm^{-1} lower than the main band center.

The observed behavior can be qualitatively explained in terms of solute−solvent interactions and particle scattering. The appearance of the sideband can be attributed to scattering: at RH near 100%, particle size grows considerably, thus making the contribution of scattering to extinction more important. Our Mie scattering calculations show that the scattering maximum for big particles ($\bar{D}_{g,0}\sim$ 0.80 μm) is at ~400 cm^{-1} to lower wavenumbers than the corresponding absorption maximum. Also, scattering contributes to the location of the main band center, shifting it towards lower wavenumbers.

At lower humidities, particle size is smaller, and the contribution of scattering is notably diminished. In this region, particles will be either liquid NaBr solutions or solid NaBr particles with pockets of concentrated NaBr solutions, as will be discussed in the next section. Although the spectra of alkali halide solutions consist only of water absorption features, it is known that spectra at different concentrations and different salts are distinguishable from one another, due to the fact that each ion pair perturbs the water molecules differently.[40] The spectra of the metal halide solutions can thus be taken as the spectra of water perturbed by the presence of the salts. The position, width, and shape of the bands will be affected by the salt ions. As RH is lowered, and thus NaBr solution concentration increases, solute−solvent interactions are stronger, producing a wavenumber increase of the band center. Indeed, the band center of 4 mol/L NaBr solutions is located ~10 cm^{-1} wavenumbers higher than the band center of pure liquid water.[30] The same trend is observed for NaCl solutions,[41] showing a 33 cm^{-1} shift between NaCl solution at 5 mol/L and pure water.

In NaCl aerosol particles, Weis and Ewing[13] measured the band centers of the OH-stretching band near 3400 cm^{-1}, and concluded that, within the uncertainty limits of ±10 cm^{-1}, the band centers were humidity independent. The behavior contrasts with that of NaBr aerosols. The higher band shifts of NaBr compared to those of NaCl can be assigned to the nature of ion-solvent interactions; as the Na^+ ion is common to both salts, the differences will be those of Cl^-−water and Br^-−water interactions. Because bromine ions are more polarizable than chlorine ions, it appears that the former interacts strongly with surrounding water molecules, thereby shifting the water absorption band more markedly than in NaCl.

Recently, it has been shown[40,42] that solution spectra of aqueous alkali halides are linear combinations of pure water spectra and salt-solvated water spectra. Water interacts with ions to form stable clusters, with the cations and anions being closely bound. For NaCl and NaBr, the clusters are made of 5 molecules of water and one pair of salt ions; these clusters are stable throughout the whole solubility range of these salts. The clusters behave as strongly bound units where the cation and anion in each cluster are inseparable. These groupings are surrounded by pure water molecules, if the solution is diluted enough. It should be noted that the ratio 5:1 of H_2O molecules to NaBr pairs roughly corresponds to the solubility of NaBr in cold water.[33]

(G) Particle Structure and Phase. Data presented in this work can be used to draw out information on particle structure, which is of interest in atmospheric chemistry. Figure 6b plots the molar ratio $n(H_2O)/n(NaBr)$ versus RH for $\bar{D}_{g,0}$= 0.24 μm diameter particles. For RH > 90%, particles quickly take up water, going from a molar ratio of 20 to about 40 at the highest RH's. This region is well above the deliquescence point, and under equilibrium conditions, particles should be NaBr aqueous solutions. This is also in agreement with thermodynamic data in Figure 6a, which show that particles yield a liquid solution of aqueous NaBr in this RH region.

For 45% < RH < 90% (from deliquescence to the onset of rapid particle growth), particle growth factors vary between 1.4 and 2.2, with $\bar{D}_g \approx 0.34-0.53$ μm. Measured water band centers are consistent with a more concentrated liquid solution of aqueous NaBr: OH-stretching band center for 4 mol kg^{-1} NaBr solutions is at 3400 cm^{-1}, but it is expected to increase with concentration. Our data indicate a NaBr concentration of 10 mol kg^{-1} in particles at RH = 80% for $\bar{D}_{g,0}$= 0.24 μm particles. Also, agreement between our experimental data and those of Cohen et al.[23] in Figure 6a support the hypothesis that aerosols are concentrated solutions in equilibrium.

For RH < 45%, infrared band centers show the highest shifts (see Figure 8) and remain quite constant in the whole interval, indicating the presence of very concentrated NaBr solutions. The infrared spectra in this region show particles with residual amounts of water. For the lowest measured RH's, we obtain a $n(H_2O)/n(NaBr)$ ratio ≈0.4, indicating the presence of solid NaBr particles plus small amounts of saturated solution (recall that $n(H_2O)/n(NaBr) > 5$ is required to dissolve NaBr in cold water). The above data suggest a particle morphology of a solid with surrounding pockets of saturated aqueous NaBr. This conclusion is similar to that for NaCl aerosols.[13]

There remains the possibility that water observed at low RH is due to liquid water adsorbed on NaBr solid surfaces. It is known that, for water adsorbed on (001) surfaces of NaCl single crystals, the band center of water is shifted ~130 cm^{-1} to higher energies over that of pure liquid water.[16] Although no similar data have been reported for NaBr, it is sensible to predict a qualitatively similar behavior. For one monolayer coverage of the Na^+Br^- surface by H_2O molecules, we may assume that, on average, each surface Na^+Br^- pair has one H_2O molecule adsorbed on it, as for sodium chloride.[13] NaBr crystals have cubic structure, similar to NaCl, with a lattice constant of 59.5 pm.[33] From these data, the surface density of Na^+Br^- pairs is calculated to be 5.7×10^{18} m^{-2}. Assuming for simplicity particles with 0.24 μm diameter, their surface area is 1.81×10^{-13} m^2, so the number of Na^+Br^- pairs onto that surface would be 1.03×10^6 sites. The number of H_2O molecules per m^3 aerosol determined in our experiment at RH = 15% is 1.77×10^{20}; as an aerosol atomizer gives $\sim 2 \times 10^{12}$ particles m^{-3}, which makes, on average, about 9×10^7 water molecules present per aerosol particle. If all water molecules were located at the surface of the particle, those figures would imply a coverage of around 90 monolayers, which excludes the possibility that water is adsorbed mainly onto the surface of particles. This conclusion follows the same trend as for NaCl aerosols.[13]

(H) Atmospheric Implications. The presented results should be taken into account in water uptake properties of sea salt aerosols. It has been pointed out that, in mixtures of NaCl and NaBr, on exposure to water, bromide segregates to surface salt, increasing the Br/Cl molar ratio by more than 1 order of magnitude.[10,11] Therefore, with Na^+Br^- ions present in considerable amount in the surface of particles, water uptake properties will influence the physical properties and heterogeneous surface chemistry of sea salt particles. Interface reactions at the surface of sea-salt particles have been suggested as an important source of halogen compounds that give rise to halogen atoms upon photolysis in the troposphere. According to Thomas et al.,[8] the reaction of NaBr aerosol particles with gaseous OH yields $Br_2(g)$ mainly in the bulk aqueous phase, and is subsequently transferred across the interface. In contrast, the reaction of surface Br^- with $O_3(g)$ at the interface was found to be the primary

source of $Br_2(g)$ under dark conditions. The influence of particle size was also studied. As expected, the contribution of small particles to interface chemistry is more important than that of larger aerosols, as the former have a larger surface-to-volume ratio. The above results suggest that interface chemistry is more likely to be important for Cl^- ions than for Br^-, given the rapid bulk-phase chemistry of Br^-, with the exception of the reaction of surface Br^- with O_3.

The presence of condensed water in salt particles and their water uptake properties is an important variable to determine the relative importance of bulk or surface chemical processes in sea-salt particles. Our results indicate that, for the smaller NaBr particles measured, only residual amounts of water are present in salt particles, unless RH is near to 100%, thus suggesting that bulk chemical reactions should have little influence. In contrast, for bigger particles the amount of water even at moderate RH makes particles to be concentrated liquid solutions, and would imply a larger contribution from aqueous bulk chemistry.

Conclusions

This work reports a characterization of NaBr aqueous aerosols by infrared extinction spectroscopy. The deliquescence and efflorescence RH's are in accordance with reported data.[23,26] Our study shows that, for RH above deliquescence point, particles begin to absorb water but do so very slowly; it is not until higher RH's (80%) that water uptake is massive. This contrasts with the behavior of NaCl aerosols, in which water absorption is very fast once the deliquescence point has been surpassed. The same behavior is observed for efflorescence: particles have lost most of their water before they reach the efflorescence point. The extension to smaller particles makes the effect dramatic: particles contain very small amounts of water unless RH is in the vicinity of 90%. Simple physical chemistry arguments support the hypothesis of solid NaBr particles with small amounts of saturated solution in pockets at low RH, whereas at high relative humidities particles are liquid aqueous NaBr solutions. Water uptake properties of sodium bromide aerosols have to be taken into account to understand the heterogeneous chemistry of marine salt aerosols.

Acknowledgment. We are grateful to MEC (Madrid) for a grant-in-aid (CGL2005-05640/CLI), to GV/EJ (Vitoria-Gasteiz) for general support through a Consolidated Research Group grant, and UPV/EHU. L.M. thanks UPV/EHU for a research grant.

References and Notes

(1) Seinfeld, J. H.; Pandis, S. N. *Atmospheric Chemistry and Physics*; John Wiley: New York, 1998.
(2) Finlayson-Pitts, B. J. *Chem. Rev.* **2003**, *103*, 4801–4822.
(3) Rossi, M. J. *Chem. Rev.* **2003**, *103*, 4823–4882.
(4) Finlayson-Pitts, B. J.; Livingston, F. E.; Berko, H. N. *Nature* **1990**, *343*, 622–625.
(5) Hunt, S. W.; Roeselova, M.; Wang, W.; Wingen, L. M.; Knipping, E. M.; Tobias, D. J.; Dabdub, D.; Finlayson-Pitts, B. J. *J. Phys. Chem. A* **2004**, *108*, 11559–11572.
(6) Frinak, E. K.; Abbatt, J. P. D. *J. Phys. Chem. A* **2006**, *110*, 10456–10464.
(7) Saiz-Lopez, A.; Shillito, J. A.; Coe, H.; Plane, J. M. C. *Atmos. Chem. Phys.* **2006**, *6*, 1513–1528.
(8) Thomas, J. L.; Jimenez-Aranda, A.; Finlayson-Pitts, B. J.; Dabdub, D. *J. Phys. Chem. A* **2006**, *110*, 1859–1867.
(9) Martin, S. T. *Chem. Rev.* **2000**, *100*, 3403–3453.
(10) Ghosal, S.; Shbeeb, A.; Hemminger, J. C. *Geophys. Res. Lett.* **2000**, *27*, 1879–1882.
(11) Zangmeister, C. D.; Turner, J. A.; Pemberton, J. E. *Geophys. Res. Lett.* **2001**, *28*, 995–998.
(12) Cziczo, D. J.; Nowak, J. B.; Hu, J. H.; Abbatt, J. P. D. *J. Geophys. Res.* **1997**, *102*, 18843–18850.
(13) Weis, D. D.; Ewing, G. E. *J. Geophys. Res.* **1999**, *104*, 21275–21285.
(14) Cziczo, D. J.; Abbatt, J. P. D. *J. Phys. Chem. A* **2000**, *104*, 2038–2047.
(15) Peters, S. J.; Ewing, G. E. *J. Phys. Chem. B* **1997**, *101*, 10880–10886.
(16) Foster, M. C.; Ewing, G. E. *J. Chem. Phys.* **2000**, *112*, 6817–6826.
(17) Gysel, M.; Weingartner, E.; Baltensperger, U. *Environ. Sci. Technol.* **2002**, *36*, 63–68.
(18) Tang, I. N.; Tridico, A. C.; Fung, K. H. *J. Geophys. Res.* **1997**, *102*, 23269–23275.
(19) Dai, Q.; Hu, J.; Salmeron, M. *J. Phys. Chem. B* **1997**, *101*, 1994–1998.
(20) Izmailov, A. F.; Myerson, A. S.; Na, H. S. *Phys. Rev. E* **1995**, *52*, 3923–3935.
(21) Myerson, A. S.; Izmailov, A. F.; Na, H. S. *J. Cryst. Growth* **1996**, *166*, 981–988.
(22) Snyder, T. D.; Richardson, C. B. *Langmuir* **1993**, *9*, 347–351.
(23) Cohen, M. D.; Flagan, R. C.; Seinfeld, J. H. *J. Phys. Chem.* **1987**, *91*, 4563–4574.
(24) Cohen, M. D.; Flagan, R. C.; Seinfeld, J. H. *J. Phys. Chem.* **1987**, *91*, 4575–4582.
(25) Cohen, M. D.; Flagan, R. C.; Seinfeld, J. H. *J. Phys. Chem.* **1987**, *91*, 4583–4590.
(26) Wise, M. E.; Biskos, G.; Martin, S. T.; Russell, L. M.; Buseck, P. R. *Aerosol Sci. Technol.* **2005**, *39*, 849–856.
(27) Bohren, C. F.; Huffman, D. R. *Absorption and Scattering of Light by Small Particles*; Wiley-VCH: Weinheim, 2004.
(28) Weis, D. D.; Ewing, G. E. *J. Geophys. Res.* **1996**, *101*, 18709–18720.
(29) Li, H. H. *J. Phys. Chem. Ref. Data* **1976**, *5*, 329–528.
(30) Rhine, P.; Williams, D.; Hale, G. M.; Querry, M. R. *J. Phys. Chem.* **1974**, *78*, 238–246.
(31) Zasetsky, A. Y.; Earle, M. E.; Cosic, B.; Schiwon, R.; Grishin, I. A.; McPhail, R.; Pancescu, R. G.; Najera, J.; Khalizov, A. F.; Cook, K. B.; Sloan, J. J. *J. Quantum Spectrosc. Radiat. Transfer* **2007**, *107*, 294–305.
(32) Downing, H. E.; Williams, D. *J. Geophys. Res.* **1975**, *80*, 1656–1661.
(33) *CRC Handbook of Chemistry and Physics*, 73 ed.; CRC Press: Boca Raton, FL, 1993.
(34) Köhler, H. *Trans. Faraday Soc.* **1936**, *32*, 1152–1161.
(35) Kreidenweis, S. M.; Koehler, K.; DeMott, P. J.; Prenni, A. J.; Carrico, C.; Ervens, B. *Atmos. Chem. Phys.* **2005**, *5*, 1357–1370.
(36) Gysel, M.; Weintgartner, E.; Baltensperger, U. *Environ. Sci. Technol.* **2002**, *36*, 63–68.
(37) *International Critical Tables of Numerical Data, Physics, Chemistry and Technology*; McGraw-Hill: New York, 1928.
(38) *American Institute of Physics Handbook*; McGraw-Hill: New York, 1972.
(39) Chen, J.-P. *J. Atmos. Sci.* **1994**, *51*, 3505–3516.
(40) Max, J.-J.; Chapados, C. *J. Chem. Phys.* **2001**, *115*, 2664–2675.
(41) Querry, M. R.; Waring, R. C.; Holland, W. E.; Hale, G. M.; Nijm, W. *J. Opt. Soc. Am.* **1972**, *62*, 849–855.
(42) Max, J.-J.; Gessinger, V.; van Driessche, C.; Larouche, P.; Chapados, C. *J. Chem. Phys.* **2007**, *126*, 184507.

JP710268R